Biosensors and Bioelectronics 55 (2014) 162–167

Contents lists available at ScienceDirect

Biosensors and Bioelectronics

journal homepage: www.elsevier.com/locate/bios

Multiplex electrical detection of avian influenza and human immunodeficiency virus with an underlap-embedded silicon nanowire field-effect transistor

Jee-Yeon Kim [a], Jae-Hyuk Ahn [a], Dong-Il Moon [a], Tae Jung Park [b], Sang Yup Lee [c], Yang-Kyu Choi [a,*]

[a] Department of Electrical Engineering, KAIST, 291 Daehak-ro, Yuseong-gu, Daejeon 305-701, Republic of Korea
[b] Department of Chemistry, Chung-Ang University, 84 Heukseok-ro, Dongjak-gu, Seoul 156-756, Republic of Korea
[c] Department of Chemical & Biomolecular Engineering, Department of Biological Sciences, Department of Bio & Brain Engineering, Bioinformatics Research Center, Center for Systems & Synthetic Biotechnology, and Institute for the BioCentury, KAIST, 291 Daehak-ro, Yuseong-gu, Daejeon 305-701, Republic of Korea

ARTICLE INFO

Article history:
Received 2 October 2013
Received in revised form
26 November 2013
Accepted 5 December 2013
Available online 12 December 2013

Keywords:
Electrical biosensor
Field-effect transistor
Underlap field-effect transistor
Avian influenza
Human immunodeficiency virus
Label-free detection

ABSTRACT

The label-free electrical detection of the binding of antibodies and antigens of avian influenza (AI) and human immunodeficiency (HIV) viruses is demonstrated through an underlap-embedded silicon (Si) nanowire field-effect transistor. The proposed sensor was fabricated on a silicon bulk wafer by a top-down process. Specifically, a Si nanowire was fabricated by a combined isotropic and anisotropic patterning technique, which is one route plasma etching process. The sensor was fabricated by a self-aligned process to the gate with tilted implantation, and it allows precise control of the underlap region. This was problematic in earlier underlap field-effect transistors fabricated by a conventional gate-last process. As a sensing metric to detect the binding of a targeted antibody, the transfer characteristic change was traced. Before and after differences between the antibody binding results were caused by changes in the channel potential on the underlap region due to the charge effect arising from the biomolecules; this is also supported by a simulation. Furthermore, the multiplex detection of AI and HIV is demonstrated, showing distinctive selectivity in each case. Thus, the proposed device has inherent benefits for the label-free, electrical, and multiplex detection of biomolecules. Moreover, its processes are compatible with commercialized technology presently used to fabricate semiconductor devices. This advantage is attractive for those involved in the construction of a point-of-care testing (POCT) system on a chip involving simple, low-cost and low-risk fabrication processes of novel structures and materials.

1. Introduction

The most important aspects of modern healthcare are the prevention of disease and appropriate treatments through early diagnosis. For effective treatment, swift and accurate diagnoses of particular diseases are essential; these requirements arouse interest in a simple and rapid on-site diagnosis system. Over the past half century, since the ion-sensitive field-effect transistor (ISFET) was introduced by Bergveld (1970), a basic structural key element based on the field-effect transistor (FET) has dominated the field of chemical and biological sensors based on the possibility of label-free detection and the potential for adaptability to signal-processing systems (Schasfoort et al., 1990a, 1990b, Bergveld, 1991; Bausells et al., 1999; Uslu et al., 2004; Yuan et al., 2011). With these approaches, however, integrating sensors and readout circuits monolithically on a chip remains a challenge.

The integrability issue can be readily overcome by adding a gate electrode, the material of which is highly compatible with the standard complementary metal-oxide semiconductor (CMOS) process (Bousse et al., 1988; Jakobson et al., 2002; Gu et al., 2009; Kim et al., 2013). Referring to the concept, a revamped FET structure termed an underlap-FET was demonstrated as a sensor for detecting antigen–antibody reactions (Lee et al., 2010). It has a gate electrode which partially covers the channel, whereas the gate entirely straddles the channel in the conventional CMOS structure. The region not covered by the gate dominantly controls the channel potential. Thus, the current flow is mostly influenced by the potential of the opened channel, leading to the use of the term underlap. An individual gate electrode for an independent sensor device is advantageous in that the sensor can be controlled separately, which is essential for sensor array processing (Baek et al., 2012) compared to a back-gate structure in that the entire

* Corresponding author. Tel.: +82 42 350 3477; fax: +82 42 350 8565.
E-mail address: ykchoi@ee.kaist.ac.kr (Y.-K. Choi).

0956-5663/$ - see front matter © 2013 Elsevier B.V. All rights reserved.
http://dx.doi.org/10.1016/j.bios.2013.12.014

wafer was used as a gate. Moreover, the underlap-FET is highly compatible with the CMOS process, implying that monolithic integration with a readout circuit and batch-fabrication at a low cost can be achieved.

The sensor performance of planar device can be improved by applying a 1-dimensional nanowire based structure due to the enhancement of gate-to-channel controllability (Singh et al., 2006; Cui et al., 2001). The miniaturization of the sensor therefore promises enhanced device performances as well as dense arrays of sensors and peripheral circuits. In other words, a Si nanowire (SiNW) wrapped by the gate will help accommodating further miniaturization of the sensor size by suppressing the short-channel effects. Nevertheless, as the previously demonstrated underlap-FET relied on the gate-last process, the fabrication method should face limitations when the underlap dimensions must be controlled precisely. Because the source and drain are formed before the patterning of the gate, the length of the underlap region critically depends on the gate alignment step (Supplementary Fig. 1a). In particular, an unreliable underlap length due to misalignment will be more critical for nano-scale devices.

Herein, we demonstrate an underlap-embedded SiNW-FET (referred to as an underlap-NWFET hereafter) fabricated by a top-down process for the label-free detection of biomolecules. To overcome the aforementioned issues, a tilted implantation process is introduced to ensure self-aligned source and drain after gate patterning (Supplementary Fig. 1b). This allows for a uniform underlap length of the NWFET. In addition, the demonstrated underlap-NWFET is fabricated on a bulk silicon substrate using a simple reactive-ion etching (RIE) technique (Moon et al., 2011) involving anisotropic and isotropic etching. This is a low-cost fabrication method compared to SiNW biosensors using silicon-on-insulator (SOI) wafers (Ahn et al., 2012). As the proposed device is based on an underlap-FET, it shares the merits of underlap-FETs and has the additional advantage of being compatible with dense arrays of sensors.

In this paper, we report the results of label-free detection tests of antibodies to verify the concept of underlap-NWFET as a biosensor. These finding are also supported by simulation data to determine the pertinent underlying mechanisms. First, the electrical characteristics of the proposed sensor are analyzed by the commercialized simulator SILVACO. Second, antigens and antibodies for the avian influenza (AI) and human immunodeficiency (HIV) viruses are used to investigate the sensitivity and selectivity of the sensor. Finally, this work is extended to the multiplex detection of different antibodies for sensor arrays. Successful multiplexed sensing of antibodies for the AI and HIV viruses is observed with proposed sensor.

2. Operating principle and simulation results

Scanning electron microscopy (SEM) images and the cross-sectional schematic of the underlap-NWFET are illustrated in Fig. 1. The sensor is composed of a source and a drain connected by a SiNW channel, which is wrapped by two separated gate and biomolecules. The source and drain were heavily doped with arsenic ion, while the underlap region ($L_{Underlap}$ in Fig. 2b) was lightly doped with boron. Biomolecules are immobilized onto the surface of the SiNW in the underlap region, which serves as a sensing site. The same bias is applied to two separate gates (G1 and G2), which are used to modulate the channel potential. Hence, the current flow is also controlled by these gates.

Here, a dominant factor influencing the current flow is the channel potential at the underlap region because the underlap region has the highest resistance throughout the SiNW due to the light doping concentration. It should be noted that the channel potential at the underlap region is sensitively modulated by the external charge arising from the immobilized biomolecules. This concept is analogous to a virtual gate which modulates the channel potential. As the first approximation, the sensor can be modeled as a simple circuit which consists of three MOSFETs (MOS1, MOS2, and MOS3) in a series, as shown in Fig. 2(a). MOS1 and MOS3 are related to the channel region with G1 and G2, and MOS2 is related to the underlap region (sensing site) with a biomolecular gate. To obtain the total drain current, it is necessary to solve each individual MOSFET equation with the condition of $I_D=I_{MOS1}=I_{MOS2}=I_{MOS3}$ according to the current conservation law and $V_{DS}=V_{DS,MOS1}+V_{DS,MOS2}+V_{DS,MOS3}$. However, when two components are connected in a series, the element with lower conductance will dominantly determine the total current. Moreover, the underlap effects influence I_{MOS1}; thus, MOS2 is also the valve of the current flow of MOS1. Therefore, the total drain current can be approximately expressed in the simple form shown below.

$$I_D(V_G,V_D,V_S)=\left(\frac{1}{I_{MOS1}(V_G,V_D,V_S)\times\beta}+\frac{1}{I_{MOS3}(V_G,V_D,V_S)}\right)^{-1} \quad (1)$$

Here, V_G, V_D, and V_S are the gate, drain and source voltages, respectively. The term β as employed here is primarily affected by the amount of charge arising from the biomolecules on the underlap region; it roughly represents the exponential relationship with the

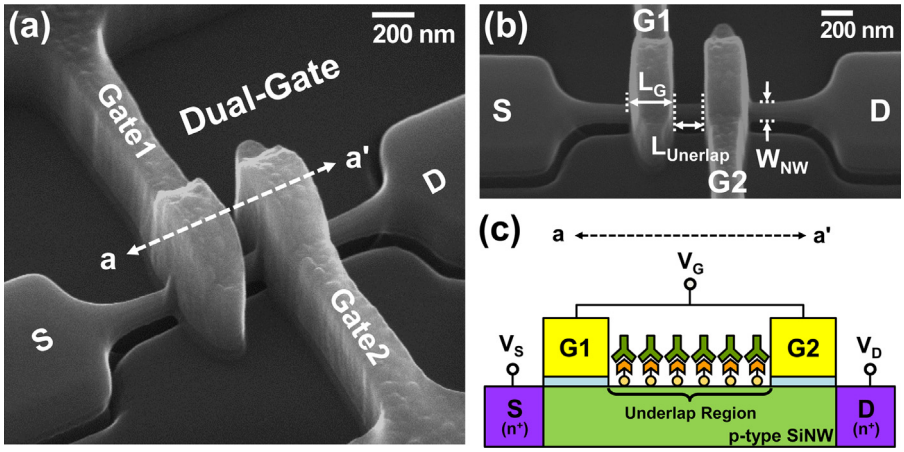

Fig. 1. SEM images and a schematic of the underlap-NWFET. (a) A tilted SEM image and (b) a top-view SEM image of the underlap-NWFET are illustrated. The device has a width (W_{NW}) of 50 nm, a gate length (L_G) of 300 nm, and underlap region ($L_{Underlap}$) of 200 nm. (c) A schematic showing an underlap-NWFET along the channel length ((a)–(a′)) direction is presented. The same gate bias, V_G, is applied to G1 and G2, and it modulates the total drain current level. The exposed channel region between G1and G2 serves as an underlap region, and biomolecules immobilized on the underlap surface affect the channel potential, resulting in a change in the drain current at a given gate bias.

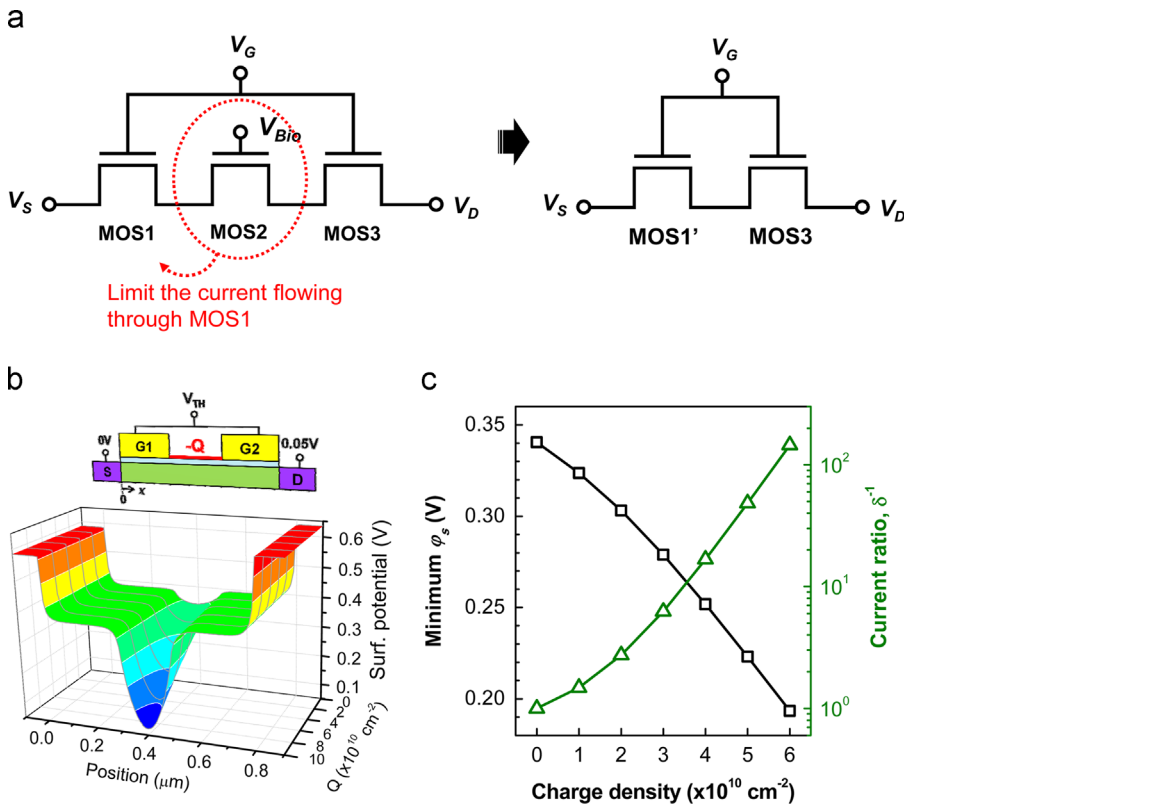

Fig. 2. Simplified equivalent circuit model for an underlap-NWFET and simulated electrical characteristics of an underlap-NWFET: (a) an underlap-NWFET can be simplified to the form of three MOSFETs connected in a series. MOS1 and MOS3 are related to the channel region covered with the gate, and MOS2 represents the underlap region. Here, charged biological species immobilized on the underlap region act as the gate potential of MOS2, and this defines I_{MOS2}. However, when two components are connected in a series, the element with lower conductance will dominantly determine the total current. Moreover, the underlap effects influence I_{MOS1}; thus, MOS2 limits the current flow in MOS1. Therefore, the total drain current can be approximately expressed in a simpler form. (b) The potential along the channel depending on the eternal charge located on the underlap region is plotted. The minimum potential is presented at the center of the underlap region; it becomes lower with a larger value of the negative charge on the underlap surface. (c) The simulated results are summarized at a gate voltage of −0.15 V, which is near the threshold voltage of the underlap-FET without a charge effect. The minimum value of the channel potential decreases, and the drain current ratio, defined as the drain current without a charge effect over the drain current with a charge effect, increases.

charge of the biomolecule attached to the underlap region. Based on this equation, it is straightforward that the first term, $I_{MOS1}\ \beta$, dominantly affects the in drain current.

The simulation is based on an underlap-NWFET with L_G of 300 nm, $L_{Underlap}$ of 200 nm, and W_{NW} of 50 nm. The simulation result of the surface channel potential depending on the surface charge of the underlap region is illustrated in Fig. 2b. The simulation is carried out at $V_{GS} = -0.15$ V, which is close to V_{TH}, with V_{DS} equal to 0.05 V. The surface channel potential on the underlap region decreases as the charge amount increases, and the channel potential has an exponential influence on the electron density. Hence, the relationship between the charge amount and the change in the drain current is expected to be exponential, as clearly shown in Fig. 2c. With a larger charge amount at the underlap region, the minimum surface potential, which dominantly affects the current, is decreased and the drain current normalized by the value without an additional charge is decreased exponentially. Here, it is important to note that the simulation results support the expectation that the proposed sensor will detect sensitive changes of charged biomolecules immobilized on the underlap surface.

3. Materials and methods

3.1. Device fabrication

The underlap-NWFET described in this paper was fabricated on a bulk Si substrate of the type commonly used as compared to silicon-on-insulator (SOI) substrate due to the low cost and long historical usage of the former. A suspended SiNW with a width of 50 nm and a height of 100 nm was fabricated using the reactive-ion etching (RIE) technique known as the Bosch process (Moon et al., 2011). The SiNW was patterned by the combined anisotropic and isotropic etching of a p-type Si wafer. Channel stop implantation was applied to suppress the leakage paths through the bulk Si, and deposition of high-density plasma (HDP) oxide along with chemical-mechanical polishing (CMP) followed to ensure device-to-device isolation. Subsequently, the SiNW – buried by the HDP oxide – was completely exposed by etching with diluted HF. The exposed SiNW was covered by thermally grown silicon dioxide (SiO_2, 7 nm), and chemically deposited poly-crystalline Si (n^+ *in situ* doped poly-Si, 350 nm). The poly-Si was patterned, and large-angle tilted implantation (45°) with arsenic ions was employed to form a source and a drain. It should be noted that an exposed channel region between two separate gates is defined here as the underlap region, which was left as an undoped channel, while the source and drain were heavily doped with the aid of a shadow effect via tilted implantation. Afterwards, dopant activation for the source and drain was performed with rapid thermal annealing at 1000 °C for 3 s. The device was subsequently annealed in forming gas ambient (H_2:N_2 = 10%:90%) to stabilize the FET characteristics. (See more details on fabrication process in the supplementary information.)

3.2. Reagents and bio-experiment procedures

The proposed underlap-NWFET was used to detect a specific antibody (anti-AI, anti-HIV) against a synthetic viral surface antigen

of both AI and HIV (AIa and HIVa). In order to help immobilize the AIa or HIVa on the underlap region, silica-binding protein (SBP) was fused with AIa or HIVa (SBP-AIa, SBP-HIVa) (Gu et al., 2009). By means of SBP, the receptors were immobilized directly onto the silica surface without extra surface modifications or treatments.

For the immobilization of receptors on the underlap region, the device was cleaned after the fabrication and then immersed at the room temperature for 1h in a phosphate-buffered saline solution, in which the receptor fused with SBP dissolved (1 × PBS, pH 7.4). The solutions, containing SBP-AIa (25 μg/ml) or SBP-HIVa (25 μg/ml), were used to functionalize the sensor for anti-AI or anti-HIV detection, respectively. The sensor was then rinsed with deionized (DI) water several times and dried with blowing N_2. Thereafter, for the specific binding of the target antibodies, the solution with the antibody was dropped onto the receptor-immobilized sensor at room temperature for 1 h. The anti-AI or anti-HIV dissolved in PBS was used for the specific binding of SBP-AIa and SBP-HIVa, whereas anti-rabbit whole Immunoglobulin G (anti-rabbit IgG) dissolved in PBS was used in non-specific binding tests with odd antibodies. Moreover, an additional step involving an interchange of the target molecules was added while handling the multiplex detection of anti-AI and anti-AI; anti-HIV was introduced onto the SBP-AIa-immobilized sensor, and anti-AI was exposed to SBP-HIVa-immobilized sensor. Washing with DI water and blow-drying with blown N_2 gas also followed.

4. Results and discussion

4.1. Current response on antigen–antibody binding

As presented in the simulation result, a charged molecular binding event on the underlap region could be read by a change in the drain current of a sensor. The drain current–gate voltage (I_D–V_G) characteristics of the sensors were measured using a semiconductor parameter analyzer (HP4156C) immediately after the aforementioned treatments. The resulting measured I_D–V_G characteristics after receptor immobilization and matched target binding are plotted on Fig. 3a and b, respectively. After binding the target antibodies, there was a clear shift in the threshold voltage (V_{TH}); for a given gate voltage, the drain current was clearly decreased. As anti-AI and anti-HIV are known to be negatively charged according to their pI values, both of which are 6.02, the channel potential of the underlap region is suppressed, decreasing the drain current. To confirm that the large reduction in the drain current was indeed caused by the specific binding between the antigen and the antibody of AI or HIV, a control experiment was conducted with anti-rabbit IgG. These results are summarized in Fig. 3c. The current ratio δ^{-1}, as expressed in Fig. 3c, is defined as the ratio of the drain current measured in the treated-receptor sensor to that in the antibody-modified sensor. Due to the non-specificity of anti-rabbit IgG with AIa or HIVa, the drain current was nearly identical before and after the anti-rabbit IgG modification step. Additionally, another control experiment using devices without an underlap region was carried out, as SBP-recombined antigens can be immobilized throughout the area where silica exists. However, there was no change; thus, any sensor region where the underlap region was excluded did not serve as a sensing site. Therefore, it was concluded that the distinct reduction of the drain current arose from the specific bindings with antigens immobilized on the underlap surface.

As shown in Fig. 4, as the concentration of the anti-AI decreased, the drain current ratio decreased. This work likely caused by the decreased charge amount of the underlap region resulting from reduced anti-AI concentration, leading to less binding between the antigen and the antibody of the AI virus. The limit of detection of the proposed underlap-NWFET was found to be 144.7 ng/ml

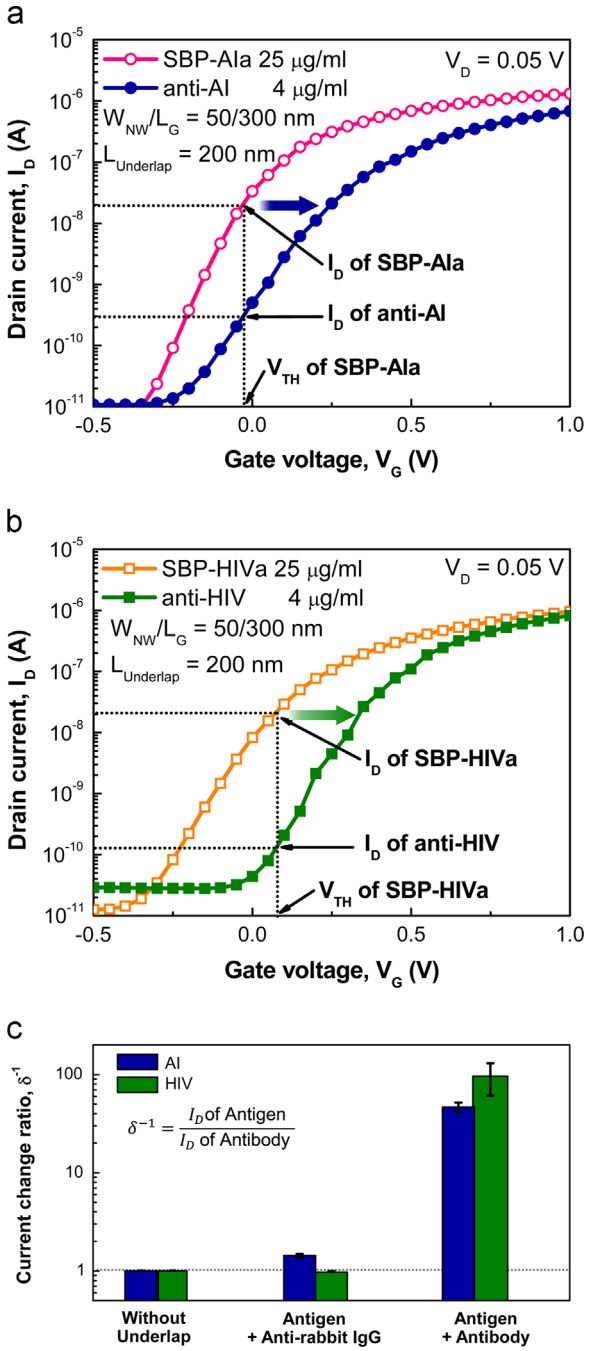

Fig. 3. Current responses of underlap-NWFETs at each step during the detection of antigen–antibody binding: (a) the I_D–V_G characteristics for the underlap-NWFET after a SBP-AIa treatment and the binding of anti-AI (4 μg/ml) are plotted, and (b) the I_D–V_G characteristics for the SBP-HIVa and anti-HIV (4 μg/ml) binding cases are plotted. In both cases, the threshold voltage shifts to the positive side, indicating a reduction of the drain current at a given voltage. (c) The results obtained for control experiments are summarized and compared with the specific binding case. The change according to non-specific binding or antigen–antibody bindings outside the underlap region is negligible compared to the change caused by the specific binding on the underlap surface.

(966.6 pmol/l). However, by optimizing the device dimensions, we believe that the sensitivity can be greatly enhanced.

4.2. Multiplex detection of antibodies

To investigate whether the proposed underlap-NWFET can be used for multiplex detection, we extended our study by adding a cross-over treatment between the antigen and antibody of the AI

and HIV viruses. The procedure for the multiplex detection test is illustrated in Fig. 5. For the SBP-AIa-immobilized sensor, anti-HIV was initially applied and the electrical characteristics of the sensor were measured. Second, anti-AI was introduced and electrical characteristics were also measured in that case as well. The same procedure was used for the SBP-HIVa-immobilized sensor; anti-AI was introduced and the measurement followed.

The measured I_D–V_G characteristics are plotted in Fig. 5a and b. As expected, fewer changes in the electrical characteristics were noted, when the SBP-AIa-immobilized sensor and the SBP-HIVa-immobilized sensor were immersed in the anti-HIV and anti-AI solutions, respectively. The I_D was decreased to 15.4 nA ($\delta^{-1}=1.3$) from 10 nA for SBP-AIa-immobilized sensor when anti-HIV was applied. For SBP-HIVa-immobilized sensor, the I_D was increased to 24.7 nA ($\delta^{-1}=0.81$) from 10 nA when anti-AI was applied. Compared to this, a remarkable change in the I_D–V_G characteristics was noted in the specific antigen–antibody binding case. For SBP-AIa-immobilized sensor, I_D was decreased to 3.83 pA ($\delta^{-1}=40.13$), and for SBP-HIVa-immobilized sensor, I_D was decreased to 4.58 pA ($\delta^{-1}=53.97$). These results are summarized in Fig. 5c and d in terms of the drain current ratio, clearly showing that antigens of AI or HIV and antibodies of AI or HIV can be selectively detected. Thus, the results indicate that the proposed underlap-NWFET can be extended for use in the multiplex detection of a broad range of biological species with the proper surface receptor.

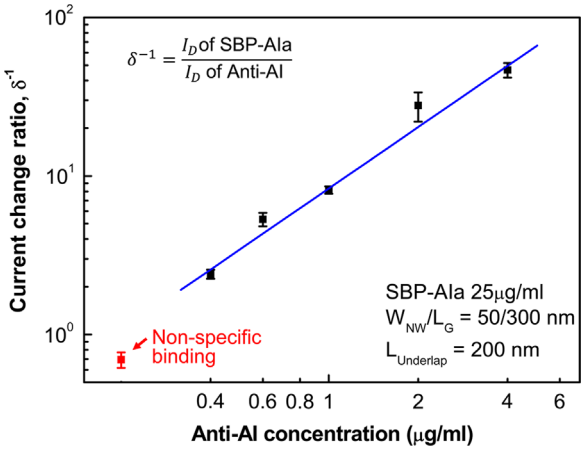

Fig. 4. Current ratio as a function of the AI antibody concentration. When the concentration of anti-AI decreased, the drain current ratio also decreased. Due to the non-specific binding, a current change occurs even without target molecules. Therefore, the limit of detection is where the non-specific and specific binding cannot be distinguished. The concentration at which the detection is limited is calculated by extrapolation.

5. Conclusions

In summary, we have developed an underlap-NWFET with a nano-scale 3-D transistor structure by used of the 1-D SiNW compared to a conventional 2-D underlap-FET. Applying nanoscale three-dimensional structure promises improved sensor performance as well as higher packing density. The proposed self-aligned gate-first process with a tilted implantation method allows precise control of the underlap region on the SiNW, compared to the gate-last process applied for the conventional planar structure. The underlap was defined as the region between two separate gates (dual-gate) covering the SiNW. The dimensions of the underlap length were precisely controlled by the patterned dual-gate with tilted implantation. In addition, the demonstrated sensor was fabricated on a bulk Si substrate by a top-down process with a combination of anisotropic and isotropic etching. The fabrication of the bulk Si wafer will enhance the degree of adaptability of sensor arrays with readout and control circuitry and lower the manufacturing cost compared to a silicon-on-insulator (SOI) wafer.

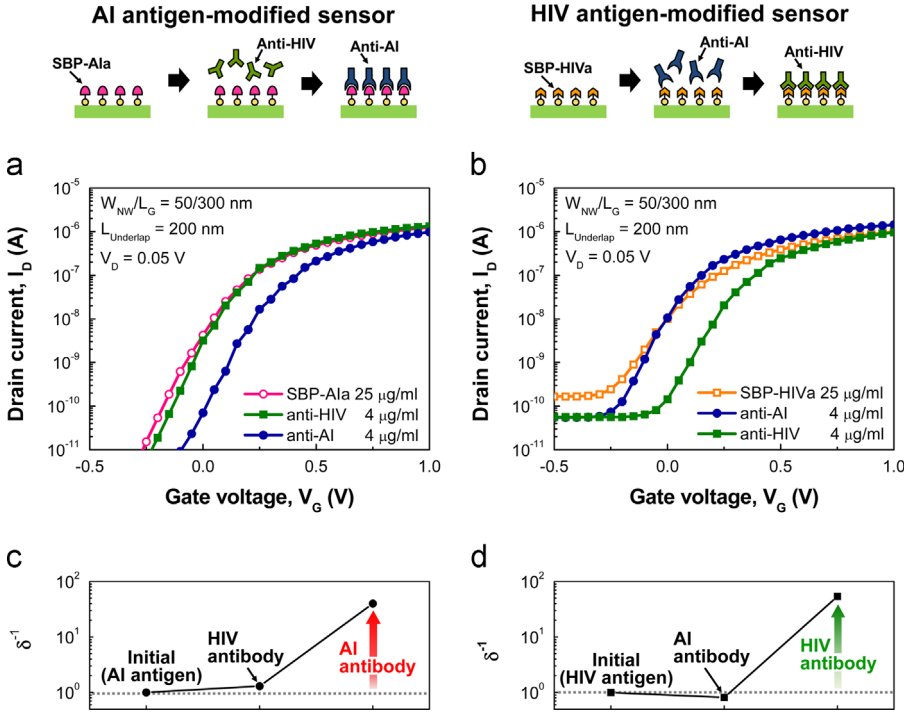

Fig. 5. Current response while the multiplex detection of AI and HIV antibodies is carried out: (a) the I_D–V_G characteristics of the SBP-AIa-immobilized sensor before antibody treatment and after the introduction of anti-HIV (4 μg/ml), and the binding of anti-AI (4 μg/ml) are shown. Additionally (b) the I_D–V_G characteristics of the SBP-HIVa-immobilized sensor before antibody treatment and after the introduction of anti-AI (4 μg/ml) and the binding of anti-HIV (4 μg/ml) are shown. In both cases, the drain currents clearly decreased when specific antibodies were introduced. (c) The results of the AI antigen-modified and (d) the HIV antigen-modified sensors are summarized. High selectivity for the multiplex detection of AI and HIV antibodies using the underlap-NWFET is clearly shown.

The proposed sensor was demonstrated for the selective electrical detection of the binding of the antigens and antibodies of AI and HIV. The sensor exhibited reproducible specific detection of the antigen–antibody binding of AI and HIV as well as high specificity with odd antibodies, proving its feasibility for used in the multiplex detection of other proteins, DNA, and cancer markers. The underlap-NWFET will allow the construction of diagnosis systems with multiple sensor arrays that are simpler, faster, and more cost-efficient given its advantages of label-free electrical detection and compatibility with commercialized silicon technology.

Acknowledgements

This work was supported by the Center for Integrated Smart Sensors funded by the Ministry of Education, Science and Technology as Global Frontier Project (CISS-2011-0031848) and the National Research and Development Program (2005-2001274) for the development of biomedical function monitoring biosensors.

Appendix A. Supplementary material

Supplementary data associated with this article can be found in the online version at http://dx.doi.org/10.1016/j.bios.2013.12.014.

References

Ahn, J.-H., Kim, J.-Y., Choi, K., Moon, D.-I., Kim, C.-H., Seol, M.-L., Park, T.J., Lee, S.Y., Choi, Y.-K., 2012. IEEE Trans. Electron. Device 59, 2243–2249.
Baek, D.J., Choi, S.-J., Ahn, J.-H., Kim, J.-Y., Choi, Y.-K., 2012. IEEE Trans. Elecron. Device 59, 2507–2511.
Bausells, J., Carrabina, J., Errachid, A., Merlos, A., 1999. Sens. Actuators, B 57, 56–62.
Bergveld, P., 1970. IEEE Trans. Biomed. Eng. BME 17, 70–71.
Bergveld, P., 1991. Biosens. Bioelectron. 6, 55–72.
Bousse, L., Shott, J., Meindl, J.D., 1988. IEEE Electron. Device Lett 9, 44–46.
Cui, Y., Wei, Q., Park, H., Lieber, C.M., 2001. Science 293, 1289–1292.
Gu, B., Park, T.J., Ahn, J.-H., Huang, X.-J., Lee, S.Y., Choi, Y.-K., 2009. Small 21, 2407–2412.
Jakobson, C.G., Dinnar, U., Feinsod, M., Nemirovky, Y., 2002. IEEE Sens. J. 2, 279–287.
Kim, C.-H., Ahn, J.-H., Kim, J.-Y., Choi, J.-M., Lim, K.-C., Park, T.J., Heo, N.S., Lee, H.G., Kim, J.-W., Choi, Y.-K., 2013. Biosens. Bioelectron. 41, 322–327.
Lee, K.-W., Choi, S.-J., Ahn, J.-H., Moon, D.-I., Park, T.J., Lee, S.Y., Choi, Y.-K., 2010. Appl. Phys. Lett. 96, 033703.
Moon, D.-I., Choi, S.-J., Kim, C.-J., Kim, J.-Y., Lee, J.-S., Oh, J.-S., Lee, G.-S., Park, Y.-C., Hong, D.-W., Lee, D.-W., Kim, Y.-S., Kim, J.-W., Han, J.-W., Choi, Y.-K., 2011. IEEE Electron. Device Lett 32, 452–454.
Schasfoort, R.B.M., Bergveld, P., Kooyman, R.P.H., Greve, J., 1990a. Anal. Chem 238 (323–329).
Schasfoort, R.B.M., Kooyman, R.P.H., Bergveld, P., Greve, J., 1990b. Biosens. Bioelectron. 5 (103–124).
Singh, N., Agarwal, A., Bera, L.K., Liow, T.Y., Yang, R., Rustagi, S.C., Tung, C.H., Kumar, R., Lo, G.Q., Balasubramanian, N., Kwong, D.-L., 2006. IEEE Electron. Device Lett 27, 383–386.
Uslu, F., Ingebrandt, S., Mayer, D., Bocker-Meffert, S., Odenthal, M., Offenhausser, A., 2004. Biosens. Bioelectron. 19, 1723–1731.
Yuan, H., Kwon, H.-C., Yeom, S.-H., Kwon, D.-H., Kang, S.-W., 2011. Biosens. Bioelectron. 28, 434–437.